13B.8

USING SHAPE METRICS TO COMPARE OBSERVED AND SIMULATED REFLECTIVITY DURING THE LANDFALL OF HURRICANE ISABEL (2003)

Corene J. Matyas *, Stephanie E. Zick, Jingyin Tang
University of Florida, Gainesville, Florida

1. INTRODUCTION

Measuring changes in the spatial attributes of precipitating regions within tropical cyclones (TCs) as they move over land facilitates the tracking of their location and how they change in size and shape. Observationally, the high spatial and temporal resolution data produced by ground-based radars permit the calculation of shape metrics of compactness (e.g., MacEachren 1985) to quantify changing storm structure over land (Matyas 2007, 2008; 2009, 2010). In this study, we use the method of Tang and Matyas (2016) to construct a 3D mosaic of Level II radar reflectivity values from the Weather Surveillance Radar 1988 Doppler (WSR-88D) network and calculate a measure of dispersion to determine how the positions of rainbands evolve during landfall of Hurricane Isabel (2003) and its subsequent transition into an extratropical cyclone.

Much can also be learned about structural changes within TCs and TC interactions with the surrounding environment by conducting model simulations. The Weather Research and Forecasting model (WRF) is widely employed for TC research studies (e.g., Davis et al. 2008; Gentry and Lackmann 2010; Torn and Davis 2012). In this study, we use WRF to model the rainband structures of Hurricane Isabel and compare model results to those observed by the WSR-88D network. As the development of a TC is sensitive to model physics (Davis et al. 2008; Fierro et al. 2009), we take an ensemble approach in selecting two different cumulus parameterizations and three microphysics schemes. We expect the storm structure to evolve differently given these different setups.

The goal of this study is to demonstrate how shape metrics can be used to compare observations and simulations of TC rainbands during landfall. To best match the observed rainband shapes to those in the simulations, we also identify and account for biases in radar reflectivity values. We emphasize that it is beyond the scope of this study to account for how differences in rainband structures evolve during the simulations, or determine which model setup performs the "best."

There are four reasons that we select Isabel for our analysis. First, it was large in size so that our innermost 3 km WRF grid should capture eyewall processes reasonably well (Gentry and Lackmann 2010). Second, operational forecast models had good predictions of track and extent of rainfall (NOAA 2003), so we expect that a research-grade simulation should initialize and perform well. Third, Isabel made landfall as a Category 2 storm at Drum Inlet, NC, on Sep. 18 at 1700 UTC (Lawrence et al. 2005), and there is adequate availability of WSR-88D data while the storm is over land. Fourth, Isabel was declared post-tropical at 1200 UTC on Sep. 19 while its center was still over the U.S., thus providing an opportunity to measure changes in the position of rainbands during the extratropical transition (ET) process.

2. WRF MODEL SETUP

In this study, we utilize the Advanced Research Weather Research and Forecasting (WRF-ARW) model version 3.6.1 (Wang et al. 2012). The WRF model solves the fully compressible, non-hydrostatic Euler equations using a mass-based terrain-following vertical coordinate (Skamarock et al. 2008). The model domain has a triple nest with a course domain of 27 km horizontal resolution and two inner nests of 9 and 3 km resolution (Fig. 1). All nests include 40 vertical levels and a model top of 2 hPa. We utilize the Yonsei University planetary boundary layer scheme (Hong et al. 2006), Rapid Radiative Transfer Model for longwave and shortwave radiation, and Noah land surface model for land surface physics (Chen and Dudhia 2001). Sea surface temperatures are prescribed. The operational National Centers for Environmental Prediction (NCEP) Global Forecast System (GFS) final analysis is used for

* *Corresponding author address:* Corene J. Matyas, Univ. of Florida, Dept. of Geography, Gainesville, FL 32611-7315; e-mail matyas@ufl.edu

the initial and boundary conditions of the simulation. The coarse domain is initialized at 0000 UTC Sep. 16, and the inner nests are initialized 24 hours later. All simulations are integrated through 0000 UTC Sep. 20 to fully encompass the landfall period and transition to an extratropical cyclone.

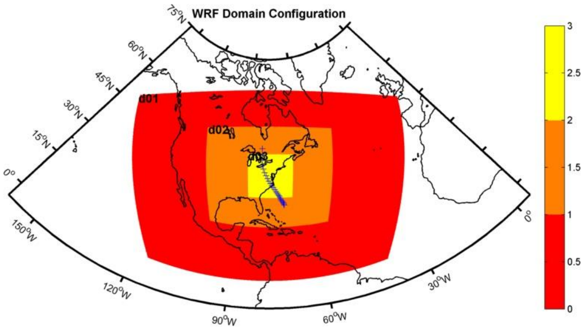

Fig. 1 WRF domain configuration and best track positions for Isabel (2003).

Modeling of tropical cyclones is known to be highly sensitive to physical processes (e.g., Davis and Bosart 2002). To force the model to produce varying rainband configurations, we use two different cumulus parameterizations for the 27 and 9 km simulations, while the innermost domain is fully explicit. Allowing the outermost grid to begin 24 hours in advance of turning on the inner nests should facilitate the development of different rainband positions desired for our shape metric calculations. We employ the modified Tiedtke (Tiedtke 1989; Zhang et al. 2011) and Kain-Fritsch (Kain and Fritsch 1990; Kain 2004) cumulus parameterizations as they have been employed both operationally and in research studies of tropical cyclones. Torn and Davis (2012) utilized both to examine biases in TC position over the Atlantic Ocean, finding that smaller temperature and wind biases in Tiedtke produced less error in track forecasts. Additionally, Tiedtke is recommended for hurricane simulations in the WRF 3.6.1 documentation.

The calculation of simulated reflectivity depends on the model's microphysics scheme (Koch et al. 2005). Thus, this research considers an ensemble of simulations with varying microphysics. We utilize three schemes that have six mass variables (water vapor, cloud droplets, cloud ice, rain, snow, and graupel), but increase in complexity with number concentration variables and their representation of cloud physical processes. The most simple parameterization is the WRF 6-class single moment (WSM6) scheme (Hong et al. 2006), which is used operationally and in numerous TC research studies. The WRF 6-class double moment (WDM6) scheme (Lim and Hong 2010) includes number concentrations for cloud and rainwater and cloud condensation nuclei. Nolan et al. (2013) employ WDM6 for the hurricane nature run. For a scheme that is fully double moment, we select Morrision-2M (Morrison et al. 2009). It predicts the mixing ratios and number concentrations of cloud droplets, cloud ice, snow, rain, and graupel. WRF simulations utilizing these three parameterizations were compared to observations taken by dual-polarized WSR-88D radars for two hurricanes during 2014 by Brown et al. (2016). They found that WSM6 and Morrison simulations produced higher reflectivity values while the WDM6 simulations had higher frequencies of small drops than were observed by the WSR-88D units.

3. RADAR ANALYSIS

As detailed in Tang and Matyas (2016), we employ a map-reduce framework (Lakshmanan and Humphrey 2014) to process Level II reflectivity data from radars within 600 km of the storm center. We construct our system using the concept of an actor model and implement it with Apache Spark using Scala programming language. All inputs, intermediate results and outputs are represented as key-values pairs. This allows us to chain multiple map and reduce functions in a pipeline to operate on complex tasks in map-reduce jobs. The complete procedure includes four steps: preprocess, map function chain, reducing function chain and post-process.

After quality control and pre-processing, data are gridded at 3 km x 3 km x 0.5 km resolution every 10 minutes using data from a 10-minute moving window. Values for grid cells with data from multiple radars are calculated by retaining the highest reflectivity value. Cells with missing values are filled using a distance-weighted interpolation performed in a Geographic Information System (GIS). We then draw contours every 5 dB*Z*, execute a smoothing algorithm, and convert the contours into polygons before calculating shape metrics.

Specific to our analysis of Isabel, data from the station located at Wilmington, North Carolina were not available during our study period. To limit the spatial extent of the model output to that of the available WSR-88D network, we create a mask layer in GIS for Sep. 18 and 19 (Fig. 2). All area and shape metric calculations are performed only on data present inside of the boundary. Although both the radar and our WRF inner nest simulation are produced at a 3 km resolution, their grid cells do not precisely align. Therefore, we place both on an identical grid at 3.5 km resolution.

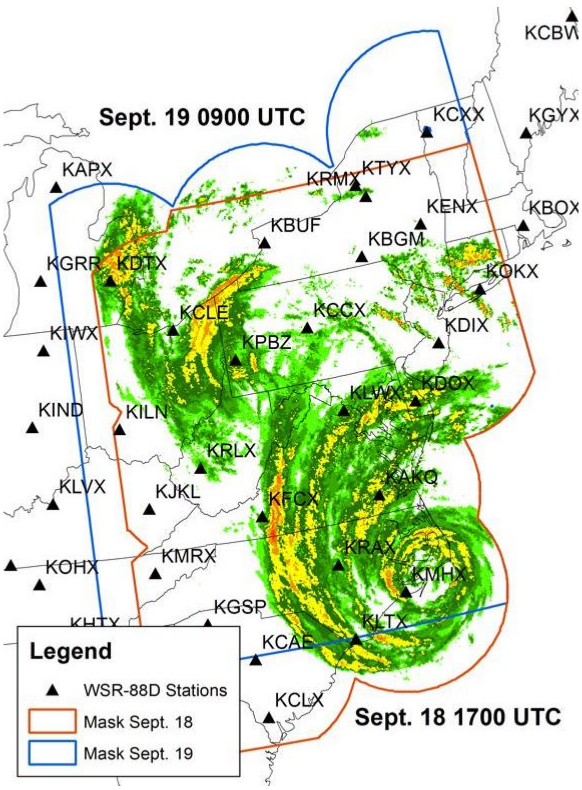

Fig 2. Mosaicked reflectivity at 3.5 km altitude with 3.5 km grid spacing at time of best track landfall and three hours prior to being declared post tropical. Data are only analyzed if inside the boundary of the mask layer.

4. MODEL POSITION AND INTENSITY COMPARISONS

We first examine plots of the best track (BT) positions for Isabel with the location of minimum sea level pressure for each of the models (Fig. 3). At the time of model initialization, Isabel's center developed slightly right of the BT position in all models and this offset continued until after landfall. The Kain-Fritsch/Morrison produced the landfall point that most closely approximates that of the BT. The simulated TC moved slightly left and had a landfall point that was approximately 10 km away from the official location of Drum Inlet, NC, and one hour behind. Due to the orientation of the barrier islands, the model landfalls occurred approximately one hour before best track at 1600 UTC on Sep. 18. The remaining five models exhibited landfalls 60-85 km northeast of the official BT landfall point. Storm forward motion slows in the model outputs as the minimum sea level pressure center moves over Virginia. At 0900 UTC Sep. 19, the BT position is near the borders of Pennsylvania, West Virginia, and Maryland. While the Kain-Fritsch/WSM6 and WDM6 positions are 45 and 80 km southeast, the Kain-Fritsch/Morrison position is 175 km south. Approximately 60 km separates the three Tiedtke positions.

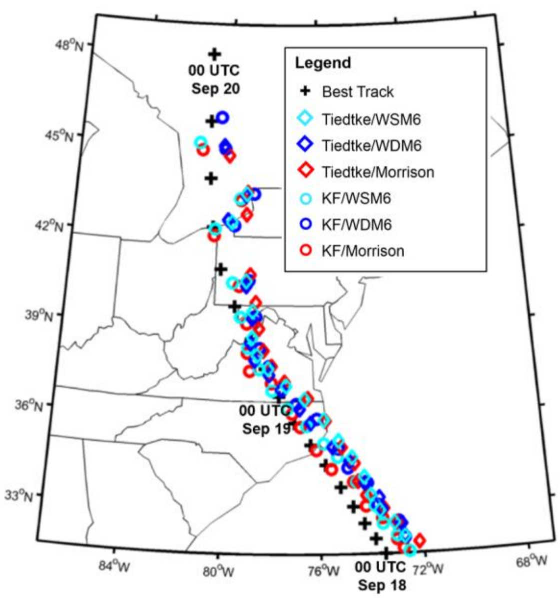

Fig. 3. Three-hourly positions of best track and WRF minimum sea level pressure.

In terms of intensity, none of the models deepen the minimum central pressure enough, but the Kain-Fritsch simulations have the lowest pressures 12-24 hours before landfall (Fig. 4.). The Tiedtke/WSM6 simulated TC intensifies in the 18 hours prior to landfall and has an intensity closest to BT at the time of landfall. After landfall, five of the six models depict the weakening of Isabel well, however, the Kain-Fritsch/Morrison simulation does not weaken the storm as much as the other models and the BT. In looking at both the position and intensity plots, we determine that all six models performed reasonably well and are considered in the next phase of the analysis.

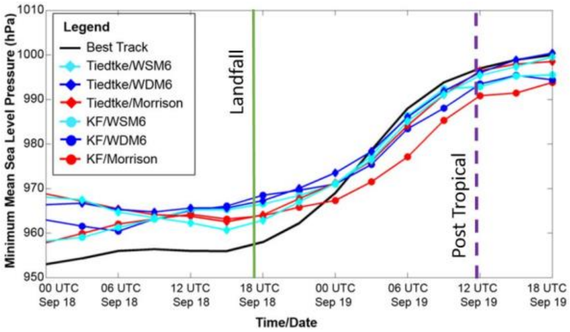

Fig. 4. Three-hourly data for minimum sea level pressure indicating time of best-track landfall 1700 UTC Sep. 18, and time declared post tropical at 1200 UTC Sep. 19.

5. REFLECTIVITY BIAS

Next, we apply a mask to the model simulated reflectivity so that the same areal coverage is available as when using the NEXRAD network. Within the boundary of the mask, we calculate the areas occupied by reflectivity values ranging from 15 – 50 dB*Z* for the observed and modeled datasets. This analysis is performed every three hours from 1200 UTC Sep. 18 – 1200 UTC Sep. 19 (Fig. 5).

The optimum window for analysis occurs when most of the TC is within range of the WSR-88D network. When the east side of the TC is out of radar range at 1200 UTC Sep. 18, the areas occupied by lower reflectivity values are much lower (~200,000 km^2 for 15 dB*Z* in the observed dataset) as compared to three hours later. This suggests that data at this time might not be the best representation of reflectivity distribution. Areas begin to decrease for the observed radar beginning at 0900 UTC through 1200 UTC Sep. 19 as the northernmost edge of the rain field moves out of radar range into Canada (Fig. 9b). However, the model areas do not exhibit as much of a decrease as the simulated TCs moved slower during this period, allowing more of their rain fields to remain within the study region.

When examining the output at each time, one obvious and consistent pattern is that both WDM6 simulations produced relatively small amounts of reflectivity values between 15-35 dBZ. In fact, total area of 15 dB*Z* never reached above 150,000 km^2. The slope of the curve is much flatter when compared to those of the observed and other 4 models. This suggests that the WDM6 microphysics scheme is under-representing stratiform precipitation, a result that compares well with that of Brown et al. (2016). A visual inspection of reflectivity at 1800 UTC Sep. 18 (Fig. 5a) shows that the moat region separating the outer rainbands from the inner core is much larger in the WDM6 simulations, and the Kain-Fritsch simulation in particular displays much less precipitation in the outer rainbands. Eighteen hours later, no reflectivity values at 35 dB*Z* or above remain within 200 km of the center in the WDM6 simulations, whereas the other simulations and the radar observations continue to exhibit these values in the region (Fig. 5b).

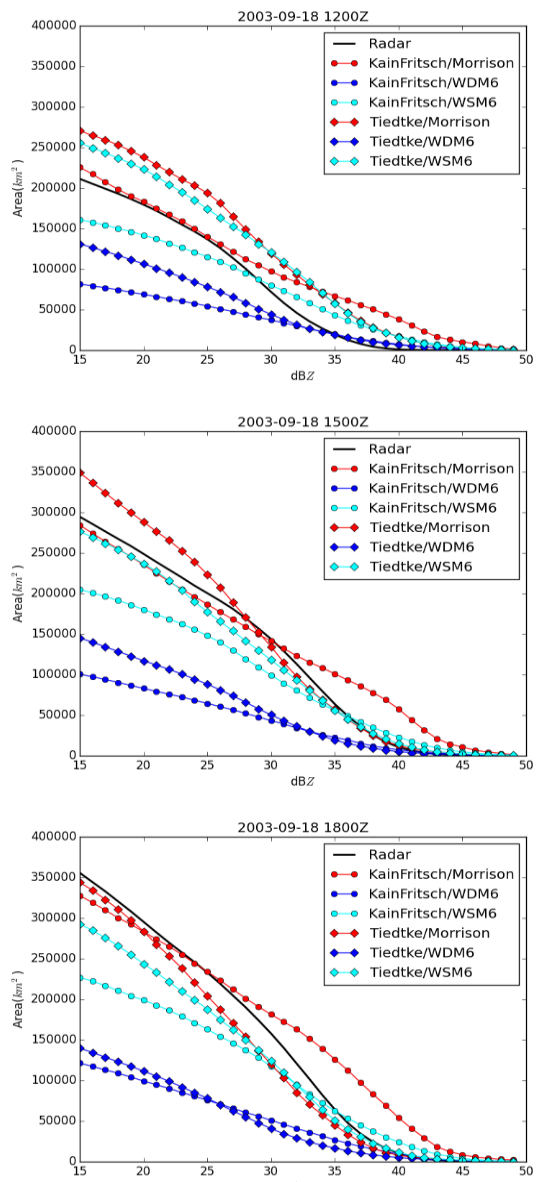

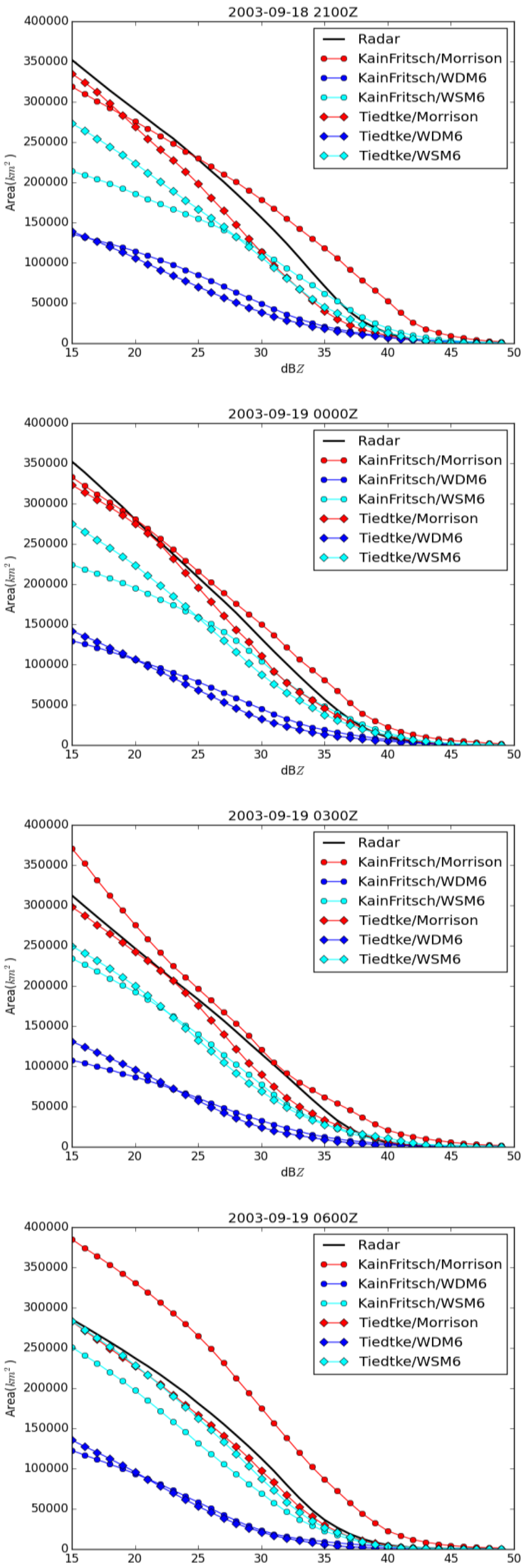

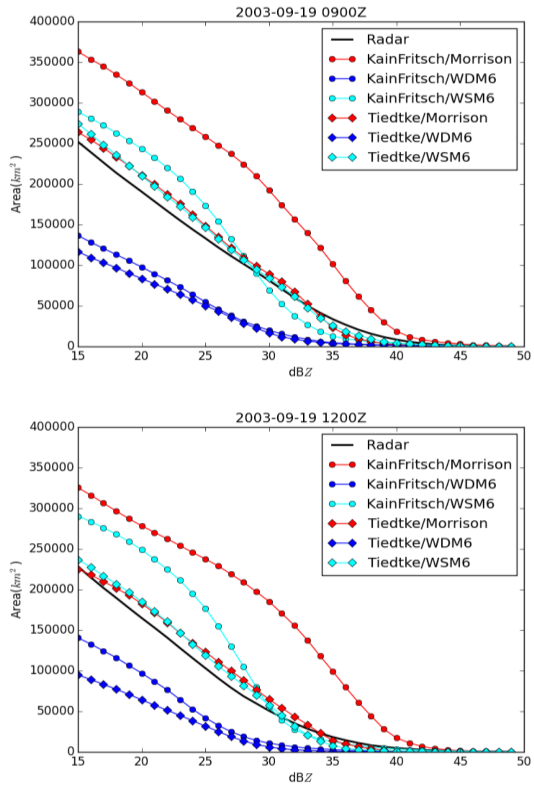

Fig 5. Area covered by each reflectivity value 15 – 50 dB*Z* every three hours from 1200 UTC Sep. 18 – 1200 UTC Sep. 19. Black line is the observed radar, cyan is WSM6, blue is WDM6, and red is Morrison. Tiedtke are diamonds, while Kain-Fritsch are circles.

The other clear result is that the areas of high reflectivity are too large in the Kain-Fritsch/Morrison simulation. This pattern is consistent across all time periods. In Fig. 5a, this simulation produced too large of an inner core with reflectivity values located 150 – 300 km from the storm center that are much higher than the observed radar or other simulations. From 0600 – 1200 UTC Sep. 19, this simulation produced high reflectivity areas across the entire range of reflectivity values we examined (Fig. 4). These larger areas of reflectivity are visible in Fig. 5b. Given its slower forward motion and relatively low values for minimum sea level pressure, it is possible that this simulation did not adequately represent the process of ET.

a.

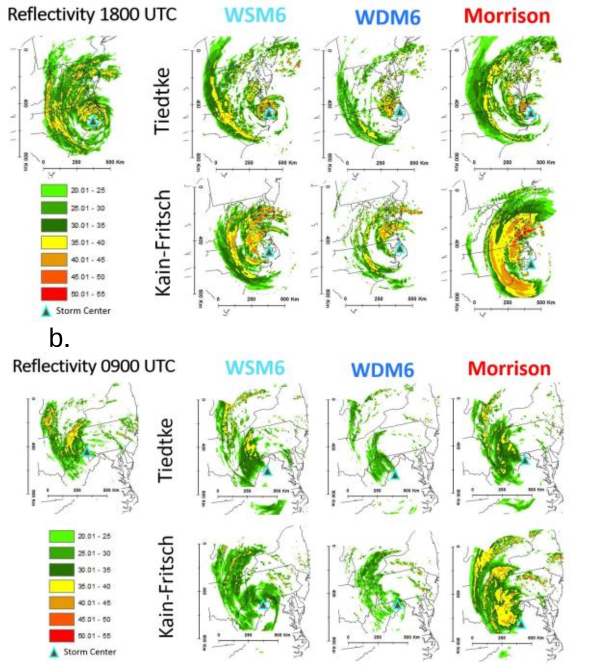

Fig 6. Reflectivity at 3.5 km altitude for WSR-88D and six WRF simulations at a) 1800 UTC Sep. 18 and b) 0900 UTC Sep. 19.

Conversations with researchers at conferences revealed the opinion that models tend to produce reflectivity values that are approximately 5 dBZ too high compared with radar observations. In our recent work (Matyas et al. 2015), we only examined 40 dB*Z* values, but concluded that a bias of approximately 4-5 dB*Z* existed in our early simulation of Hurricane Isabel when compared to radar observations. An examination of Fig. 4 reveals an important finding in regards to the reflectivity bias. Besides the fact that the bias varies across the models, it also varies across the range of dB*Z* levels, with values farther from observed at lower reflectivity values, and closest to observed at 35 or 40 dB*Z*. When averaging values across all nine times for each model compared to the observed reflectivity every 5 dBZ, the majority of models under-estimate the lower reflectivity values, and over-estimate the higher values (Table 1).

The model that comes closest to supporting the notion that most simulations tend to overestimate reflectivity by 5 dB*Z* is the Kain-Fritsch/Morrison run, with values 2 dBZ higher for 20-25 dB*Z*, and 4 dB*Z* higher 30-40 dB*Z*. The extremely low values for both WDM6 runs are apparent, yet they still over estimate by 1-2 dB*Z* at 45 dB*Z*. The Tiedtke/Morrison simulation has the least bias at each reflectivity level, yielding the lowest average bias across all times for all levels, and Tiedtke/WSM6 is a close second. Given the relatively poor performance of the WDM6 simulations, we do not include them in next part of the study. For the four remaining models, we apply the bias correction for each corresponding reflectivity value listed in Table 1 prior to calculating the dispersion metric in the next section.

Table 1. Averaged reflectivity bias for each WRF model.

Refl.	T/ WSM6	T/ WDM6	T/ Morr	KF/ WSM6	KF/ WDM6	KF/ Morr
20	-2.3	-10	1	-7.1	-10	1.9
25	-1.9	-14.3	0	-6.3	-14.4	1.8
30	-1.4	-12.5	-0.4	-2.3	-13.6	4
35	-1	-7.1	-0.5	-0.8	-6.8	4.1
40	0.8	-3.1	1.4	1.8	-1.8	4.5
45	2.4	1.4	1.8	3.8	2.6	6.5
Avg.	-0.6	-7.6	0.5	-1.8	-7.3	3.8

6. DISPERSION METRIC

Finally, we consider the spatial distribution of reflectivity values by calculating a measure of their dispersion. Our goal is to demonstrate that this measure of compactness (MacEachren 1985; Wentz 2000; Li et al. 2014) can quantify the different spatial patterns of rainfall produced by the models when compared to the observed radar. Furthermore, this metric can reveal the time at which rainfall becomes more dispersed away from the storm center as Isabel undergoes ET. First, we convert the reflectivity areas into polygons that enclose values of 20 dB*Z* and higher, 25 dB*Z* and higher, etc. up to 40 dB*Z*. We calculate the center of mass and its distance from the TC's circulation center, omitting polygons smaller than 48 km^2. Many studies employ a 500 km search radius (Larson et al. 2005; Villarini et al. 2014; Hernández-Ayala and Matyas 2016), however TCs tend to expand as they more poleward (Chan and Chan 2013; Guo and Matyas 2016). For this reason, we employ a 600 km search radius as in Zick and Matyas (2016) to avoid including rainfall associated with other systems.

In the dispersion metric (Equation 1) the distance of the polygon centroid from the storm center ($r_{centroid}$) is divided by the 600 km search radius (r_{search}) so that polygons located near the boundary of the search radius have a high value. Additionally, each polygon is weighted by its size so that larger polygons have a higher contribution in the final value. The overall metric produces values from 0-1, with one being highly dispersed to the edges of the search radius. We expect a TC undergoing ET to lose convection within its inner core and its rain fields to expand poleward of the storm center (Harr and Elsberry 2000; Klein et al. 2000; Jones et al. 2003; Matyas 2008; Zick and Matyas 2016). Thus dispersion should increase until the rain fields move beyond radar range.

$$D=\sum_{i=1}^{NP}\frac{Area_i}{\sum_j^{NP} Area_j}\left(\frac{r_{centroid,i}}{r_{search}}\right) \quad (1)$$

When comparing the images in Figures 5a and 5b, it appears that the cumulus parameterization does have an effect on the overall storm shape. The Tiedtke simulations feature an inner core that more closely matches that of the radar observations with smaller radius to the eyewall. However, the outer rainbands are in a spiral shape that is too broad compared to the radar observations at 1800 UTC. At the same time, the Kain-Fritsch simulations depict a large eyewall diameter and less precipitation in the outer rainbands. The larger areas of precipitation farther outward from the center in the Tiedtke simulations should produce a higher dispersion value when compared to the Kain-Fritsch simulations and the observed radar.

Upon examining the hourly time series of dispersion (Fig. 6), it is clear that accounting for the reflectivity bias brings the model results into fairly good agreement. The Kain-Fritsch/WSM6 simulation produces dispersion values that were consistently lower than the other models and the observed radar for 20-30 dB*Z*, while both Tiedtke simulations are very similar to one another with values slightly higher than the radar observations. Another finding is that most values start to drop around 0900 UTC. As seen in Fig. 5b, the northernmost edge of the rain field begins to move out of radar range, effectively limiting the centroid radius to values lower than the search radius, which forces the metric values to drop.

When dispersion values occurring after 0900 UTC are removed from consideration for the observed radar data, dispersion increases through time with a slope approximating 0.37. This trend does not occur in the Tiedtke simulations until reaching higher reflectivity values of 35 and 40 dB*Z*. The ensemble members and observed reflectivity have the most similar values of dispersion when considering polygons bounded by 35 dB*Z*. This is also where reflectivity has the lowest bias in some of the simulations. On the other hand, the greatest spread is in the 40 dB*Z* polygons. Values from the radar observations are higher than the models in the beginning of the period, and dispersion increases the most dramatically between 0000 and 0600 UTC for all five cases. Also, the two Tiedtke simulations produce lower values in the beginning, then exhibit the highest values after 0500 UTC. This supports the earlier observation that the Tiedtke simulations have more convection in the storm's inner core in the beginning, and after these regions erode, the remaining high reflectivity regions are located in the outer rainbands on or near the edge of the search radius. The increase in dispersiveness for Isabel while moving over Virginia supports the findings of Zick and Matyas (2016) who examined TCs from 2004-2014 in the North American Regional Reanalysis and found that dispersion increased as TCs moved over this region (their Fig. 12).

The dispersion metric also aids in examining the changes produced when utilizing different bias adjustments. We arrived at the values for Table 1 by averaging across the nine observation times displayed in Fig. 4. As discussed earlier, 1200 UTC Sep. 18 is a time when some of the storm's core is outside of the study region. If reflectivity bias from this time is removed from consideration, the bias for Tiedtke/Morrison is reduced for 40 dB*Z* so that no adjustment is needed. With this being the case, additional reflectivity regions meeting the 48 km^2 size requirement are included in the calculation of the dispersion metric, increasing (decreasing) its values in the early (late) period and bringing it more in line with the observed radar. Thus, we emphasize that the reflectivity biases should be calculated on an individual storm basis, multiple time periods need to be considered, and that a simple averaging across time may not be sufficient.

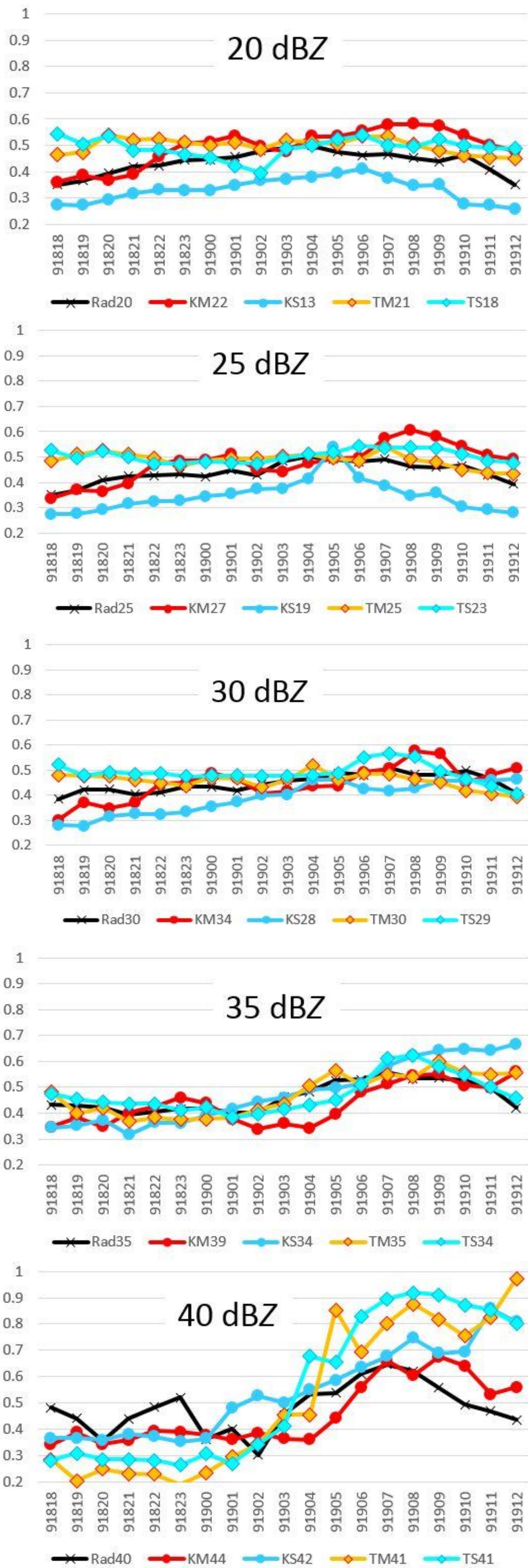

Fig 6. Dispersion metric each hour for WSR-88D (Rad) and four WRF simulations (WSM6 and Morrison for Kain-Fritsch and Tiedtke) from 1800 UTC Sep. 18 – 1200 UTC Sep. 19. Labels contain the actual reflectivity utilized considering the bias.

7. CONCLUSIONS AND FUTURE WORK

We compared radar reflectivity values observed by the WSR-88D network to simulated reflectivity values produced by an ensemble of WRF models for Hurricane Isabel (2003). Our ensemble of simulations included three different microphysics schemes each having six hydrometeor classes and ranging from single moment (WSM6), to partial double-moment (WDM6), to fully double-moment Morrison. We utilized modified Tiedtke and Kain-Fritsch cumulus parameterizations and initialized the outermost grid 24 hours prior to the inner grids to assure that the cumulus parameterization would produce different patterns of convective precipitation. We examined data at a constant altitude of 3.5 km, and masked the data so that only values within the WSR-88D network's range were examined at a given time. We compared the areas occupied by various reflectivity values to determine a bias adjustment to bring model results more in line with the radar observations. Finally, we calculated the dispersion of the rainbands at different reflectivity values across an 18-hour period while Isabel completed an ET.

All six model runs produced reasonable storm tracks and intensities although the timing of landfall and its location varied by up to one hour and 60 km from the best track. Our first comparisons to observed radar involved calculating the area occupied by each reflectivity value and revealed that the WDM6 simulations consistently under-produced stratiform precipitation, yielding a bias as large as 14 dB*Z.* These simulations were not examined further. The Kain-Fritsch/Morrison simulation produced values that were too high, especially towards the end of the simulation. This could be due to the fact that this storm did not weaken as much as it should have and its slow forward speed could mean that the ET process was not well-simulated in this run.

As hypothesized, the dispersion metric showed increases in the spread of rainfall regions away from the storm center as Isabel completed its ET. The Tiedtke simulations produced more convection in the storm's core, but also in the outermost spiral rainbands which caused dispersion values to be higher. On the other hand, the Kain–Fritsch simulations had a large eyewall with less rainfall in the outer regions of the storm, resulting in lower dispersion values, particularly in the WSM6 run. The dispersion metric adequately captured these differences.

Future research will calculate additional shape metrics to investigate other measures of storm compactness such as asymmetry, elongation, and fragmentation, and will also measure closure, or the degree to which rainbands encircle the storm's center. We will also employ shape metrics to compare model results during the entire run including the period when Isabel is out of radar range. An examination of reflectivity values at other altitudes will help determine if our selection of 3.5 km might explain the under-representation of precipitation in the WDM6 simulations. We also seek to compare the results from this study to other landfalling TCs.

8. REFERENCES

Brown, B. R., M. M. Bell, and A. J. Frambach, 2016: Validation of simulated hurricane drop size distributions using polarimetric radar. *Geophysical Research Letters*, **43,** 910-917.

Chan, K., and J. Chan, 2013: Angular momentum transports and synoptic flow patterns associated with tropical cyclone size change. *Monthly Weather Review*, **141,** 3985–4007.

Chen, F., and J. Dudhia, 2001: Coupling an advanced land surface-hydrology model with the Penn State-NCAR MM5 modeling system. Part I: Model implementation and sensitivity. *Monthly Weather Review*, **129,** 569-585.

Davis, C., and L. F. Bosart, 2002: Numerical simulations of the genesis of Hurricane Diana (1984). Part II: Sensitivity of track and intensity prediction. *Monthly Weather Review*, **130,** 1100-1124.

Davis, C., and Coauthors, 2008: Prediction of landfalling hurricanes with the Advanced Hurricane WRF model. *Monthly Weather Review*, **136,** 1990-2005.

Fierro, A. O., R. F. Rogers, F. D. Marks, and D. S. Nolan, 2009: The impact of horizontal grid spacing on the microphysical and kinematic structures of strong tropical cyclones simulated with the WRF-ARW model. *Monthly Weather Review*, **137,** 3717-3743.

Gentry, M. S., and G. M. Lackmann, 2010: Sensitivity of simulated tropical cyclone structure and intensity to horizontal resolution. *Monthly Weather Review*, **138,** 688-704.

Guo, Q., and C. Matyas, 2016: Comparing the spatial extent of Atlantic basin tropical cyclone wind and rain fields prior to land interaction. *Physical Geography*, **37,** 5-25.

Harr, P. A., and R. L. Elsberry, 2000: Extratropical transition of tropical cyclones over the western North Pacific. Part I: Evolution of structural characteristics during the transition process. *Monthly Weather Review*, **128,** 2613-2633.

Hernández-Ayala, J. J., and C. J. Matyas, 2016: Tropical cyclone rainfall over Puerto Rico and its relations to environmental and storm specific factors. *International Journal of Climatology*, **36,** 2223-2237.

Hong, S.-Y., Y. Noh, and J. Dudhia, 2006: A new vertical diffusion package with an explicit treatment of entrainment processes. *Monthly Weather Review*, **134,** 2318-2341.

Jones, S. C., and Coauthors, 2003: The extratropical transition of tropical cyclones: Forecast challenges, current understanding, and future directions. *Weather and Forecasting*, **18,** 1052-1092.

Kain, J. S., 2004: The Kain-Fritsch convective parameterization: an update. *Journal of Applied Meteorology*, **43,** 170-181.

Kain, J. S., and J. M. Fritsch, 1990: A one-dimensional entraining/detraining plume model and its application in convective parameterization. *Journal of the Atmospheric Sciences*, **47,** 2784-2802.

Klein, P. M., P. A. Harr, and R. L. Elsberry, 2000: Extratropical transition of western North Pacific tropical cyclones: An overview and conceptual model of the transformation stage. *Weather and Forecasting*, **15,** 373-395.

Koch, S. E., B. Ferrier, M. T. Stoelinga, E. Szoke, S. J. Weiss, and J. S. Kain, 2005: The use of simulated radar reflectivity fields in the diagnosis of mesoscale phenomena from high-resolution WRF model forecasts. *Preprints, 11th Conf. on Mesoscale Processes, Albuquerque, NM, Amer. Meteor. Soc., J4J*.

Lakshmanan, V., and T. W. Humphrey, 2014: A MapReduce technique to mosaic continental-scale weather radar data in real-time. *Selected Topics in Applied Earth Observations and Remote Sensing, IEEE Journal of*, **7,** 721-732.

Larson, J., Y. P. Zhou, and R. W. Higgins, 2005: Characteristics of landfalling tropical cyclones in the United States and Mexico: Climatology and interannual variability. *Journal of Climate*, **18,** 1247-1262.

Lawrence, M. B., L. A. Avila, J. L. Beven, J. L. Franklin, R. J. Pasch, and S. R. Stewart, 2005: Atlantic hurricane season of 2003. *Monthly Weather Review*, **133,** 1744-1773.

Li, W., T. Chen, E. A. Wentz, and C. Fan, 2014: NMMI: A mass compactness measure for spatial pattern analysis of areal features. *Annals of the Association of American Geographers*, **104,** 1116-1133.

Lim, K.-S. S., and S.-Y. Hong, 2010: Development of an effective double-moment cloud microphysics scheme with prognostic cloud condensation nuclei (CCN) for weather and climate models. *Monthly Weather Review*, **138,** 1587-1612.

MacEachren, A. M., 1985: Compactness of geographic shape: comparison and evaluation of measures. *Geografiska Annaler*, **67B,** 53-67.

Matyas, C. J., 2007: Quantifying the shapes of US landfalling tropical cyclone rain shields. *The Professional Geographer*, **59,** 158-172.

Matyas, C.J., 2008: Shape measures of rain shields as indicators of changing environmental conditions in a landfalling tropical storm. *Meteorological Applications*, **15,** 259-271.

Matyas, C. J., 2009: A spatial analysis of radar reflectivity regions within Hurricane Charley (2004). *Journal of Applied Meteorology and Climatology*, **48,** 130-142.

Matyas, C. J., 2010: Associations between the size of hurricane rain fields at landfall and their surrounding environments. *Meteorology and Atmospheric Physics*, **106,** 135-148.

Matyas, C. J., J. Tang, and S. E. Zick, 2015: Performing spatial analysis on tropical cyclone rainband structures after creating a 3D Mosaic of WSR-88D reflectivity data using a map-reduce framework and a Geographic Information System (GIS). *37th conference on Radar Meteorology*, Norman, OK.

Morrison, H., G. Thompson, and V. Tatarskii, 2009: Impact of cloud microphysics on the development of trailing stratiform precipitation in a simulated squall line: Comparison of one-and two-moment schemes. *Monthly Weather Review*, **137,** 991-1007.

National Oceanic and Atmospheric Administration, U. S. D. o. C.: Service Assessment: Hurricane Isabel, September 18-19, 2003. [Available online at http://www.weather.gov/os/assessments/pdfs/isabel.pdf.]

Nolan, D. S., R. Atlas, K. T. Bhatia, and L. R. Bucci, 2013: Development and validation of a hurricane nature run using the joint OSSE nature run and the WRF model. *Journal of Advances in Modeling Earth Systems*, **5,** 382-405.

Skamarock, W. C., J. Klemp, J. Dudhia, D. Gill, and D. Barker, 2008: A description of the Advanced Research WRF version 3. *NCAR Tech. Note NCAR/TN-4751STR.*

Tang, J., and C. J. Matyas, 2016: Fast playback framework for analysis of ground-based Doppler radar observations using Map-Reduce technology. *Journal of Atmospheric and Oceanic Technology*, **33,** 621-634.

Tiedtke, M., 1989: A comprehensive mass flux scheme for cumulus parameterization in large-scale models. *Monthly Weather Review*, **117,** 1779-1800.

Torn, R. D., and C. A. Davis, 2012: The influence of shallow convection on tropical cyclone track forecasts. *Monthly Weather Review*, **140,** 2188-2197.

Villarini, G., R. Goska, J. A. Smith, and G. A. Vecchi, 2014: North Atlantic tropical cyclones and U.S. flooding. *Bulletin of the American Meteorological Society*, **95,** 1381-1388.

Wang, W., and Coauthors, 2012: User's Guide for Advanced Research WRF (ARW) Modeling System Version 3.

Wentz, E. A., 2000: A shape definition for geographic applications based on edge, elongation, and perforation. *Geographical Analysis*, **32,** 95-112.

Zhang, C., Y. Wang, and K. Hamilton, 2011: Improved representation of boundary layer clouds over the Southeast Pacific in ARW-WRF using a modified Tiedtke cumulus parameterization scheme. *Monthly Weather Review*, **139,** 3489-3513.

Zick, S. E., and C. J. Matyas, 2016: A shape metric methodology for studying the evolving geometries of synoptic-scale precipitation patterns in tropical cyclones. *Annals of the Association of American Geographers, in revision*.